Available online at www.sciencedirect.com

SCIENCE DIRECT®

Biochimica et Biophysica Acta 1663 (2004) 222–231

BIOCHIMICA ET BIOPHYSICA ACTA
BBA

www.bba-direct.com

# Characterization of the main transition of dinervonoylphosphocholine liposomes by fluorescence spectroscopy

Antti J. Metso[a], Juha-Pekka Mattila[a], Paavo K.J. Kinnunen[b,*]

[a] *Helsinki Biophysics and Biomembrane Group, Institute of Biomedicine/Biochemistry, University of Helsinki, Biomedicum, Haartmanninkatu 8, P.O. Box 63, FIN-00014, Helsinki, Finland*

[b] *Memphys-Center for Biomembrane Physics, Finland*

Received 3 October 2003; received in revised form 11 March 2004; accepted 24 March 2004

Available online 20 April 2004

**Abstract**

The structural dynamics of the main phase transition of large unilamellar dinervonoylphosphocholine (DNPC) vesicles was investigated by steady state and time-resolved fluorescence spectroscopy of the membrane incorporated fluorescent lipid analog, 1-palmitoyl-2[10-(pyren-1-yl)]decanoyl-*sn*-glycero-3-phosphocholine (PPDPC). These data were supplemented by differential scanning calorimetry (DSC) and fluorescence anisotropy measured for 1-palmitoyl-2-(3-(diphenylhexatrienyl) propanoyl)-*sn*-glycero-3-phosphocholine (DPHPC). The collected data displayed several discontinuities in the course of the main transition and the pretransition. The discontinuities seen in the fluorescence properties may require modification of the existing models for phospholipid main transition as a first order process. From our previous study on dipalmitoylphosphocholine (DPPC), we concluded the transition to involve a first-order process resulting in the formation of an intermediate phase, which then converts into the liquid crystalline state by a second order process. Changes in the physical properties of the DNPC matrix influencing probe behavior were similar to those reported previously for PPDPC in DPPC. In gel state DNPC [$(T - T_m) < -10$] the high values for excimer/monomer emission ratio ($I_e/I_m$) suggest enrichment of the probe in clusters. In this temperature range, excimer fluorescence for PPDPC (mole fraction $X_{PPDPC} = 0.02$) is described by two formation times up to $(T - T_m) \approx -10$, with a gradual disappearance of the fractional intensity ($I_{R1}$) of the shorter formation time ($\tau_{R1}$) with increasing temperature up to $(T - T_m) \approx -10$. This would be consistent with the initiation of the bilayer melting at the PPDPC clusters and the subsequent dispersion of the one population of PPDPC domains. A pronounced decrement in $I_e$ starts at $(T - T_m) = -10$, continuing until $T_m$ is reached. No decrease was observed in fluorescence quantum yield in contrast to our previous study on DPPC/PPDPC large unilamellar vesicles (LUVs) [J. Phys. Chem., B 107 (2003) 1251], suggesting that a lack of proper hydrophobic mismatch may prevent the formation of the previously reported PPDPC superlattice. With further increase in temperature and starting at $(T - T_m) \approx -1$, $I_e$, $\tau_{R2}$, and excimer decay times ($\tau_D$) reach plateaus while increment in *trans* → *gauche* isomerization continues. This behavior is in keeping with an intermediate phase existing in the temperature range $-1 < (T - T_m) < 4$ and transforming into the liquid disordered phase as a second order process, the latter being completed when $(T - T_m) \rightarrow 4$ and corresponding to ≈ 50% of the total transition enthalpy.


*Keywords:* Liposome; Phase transition; Pyrene

## 1. Introduction

Lipids represent the principal structural elements of all biological membranes and characteristically to liquid crystals exhibit a range of phases and phase transitions [2]. The significance of these properties of lipids is beginning to be recognized and phospholipid phase transitions are considered to be important in regulating the activities of membrane-associated proteins [3–7] for instance. As most cellular functions of eukaryotes apparently take place on membrane surfaces [8], elucidation of the coupling between the physical state, organization and function of biomem-

*Abbreviations:* DMPC, 1,2-dimyristoyl-*sn*-glycero-3-phosphocholine; DNPC, 1,2-dinervonoyl-*sn*-glycero-3-phosphocholine; DPHPC, 1-palmitoyl-2-(3-(diphenylhexatrienyl) propanoyl)-*sn*-glycero-3-phosphocholine; DPPC, 1,2-dipalmitoyl-*sn*-glycero-3-phosphocholine; $\Delta H$, enthalpy change; $I_e/I_m$, ratio of pyrene excimer and monomer fluorescence intensity; $^{Int}I_e$, integrated excimer intensity of the time-resolved fluorescence emission; LUV, large unilamellar vesicle; MLV, multilamellar vesicle; PPDPC, 1-palmitoyl-2[10-(pyren-1-yl)]decanoyl-*sn*-glycero-3-phosphocholine; $T$, temperature; $T_m$, main phase transition temperature; $T_p$, pretransition temperature; $X_{lipid}$, mole fraction of the indicated lipid; $\tau_R$, rise time (excimer formation time); $\tau_D$, excimer decay time; $\bar{\tau}_M$, weighted average monomer lifetime

* Corresponding author. Tel.: +358-9-19125400; fax: +358-9-19125444.

*E-mail address:* Paavo.Kinnunen@Helsinki.Fi (P.K.J. Kinnunen).

0005-2736/$ - see front matter © 2004 Elsevier B.V. All rights reserved.
doi:10.1016/j.bbamem.2004.03.014

branes is clearly of fundamental importance [3]. A large fraction of all biological membranes is believed to be in fluid state under physiological conditions. Yet, structural changes in axon membranes accompanying their excitation suggest that nerve impulse involves a transient electrostatically induced phospholipid phase transition from liquid crystalline to gel state [3]. Biomembranes are highly heterogeneous in the lateral organization on different time- and length-scales [3,4]. Importantly, membrane lateral organization is intimately connected to phospholipid phase behavior. Accordingly, dynamic organization into microdomains in membranes enriched with cholesterol and sphingomyelin with the coexistence of fluid and liquid ordered state domains has been suggested [9,10].

Dynamic lateral heterogeneity due to coexisting fluctuating gel and liquid crystalline domains accompanies the main transition of phospholipids [11–14]. Upon $T \rightarrow T_m$, the intensity of these fluctuations is enhanced and causes bending elasticity and both lateral (area) and transversal compressibilities as well as the heat capacity of the bilayer to have a maximum at $T_m$ [12,13,15–18]. The permeability maximum of bilayers and augmented activity of phospholipases $A_2$ near $T_m$ have been attributed to the length of the phase boundary [12,14,19–23] also having a maximum at $T_m$ [13].

We have recently forwarded a more detailed description of the main transition based on time-resolved fluorescence spectroscopic characterization of DPPC [1]. In brief, upon $T \rightarrow T_m$, and characteristically to a first order transition, fluid-like domains start to form in the gel phase bilayer, this fraction of the total lipid increasing with temperature and the length of the interfacial boundary increasing with the progression of the transition. In keeping with the model by Heimburg [24] the fluid-like domains would start to form in the line defects initiated at the corrugations appearing at $T_p$. However, upon approaching $T_m$, the phase boundary seems to disappear, with the formation of an intermediate phase. More specifically, the disappearance of the domain boundary was suggested to result from the properties of the coexisting fluid-like and gel phases approaching each other as two parallel second order processes developing with temperature, causing diminishing line tension and hydrophobic mismatch. This intermediate phase would then transform into the liquid disordered phase as a second order transition with weak first order characteristics due to heterophase fluctuations [25], with further increase in acyl chain *trans* → *gauche* isomerization. Upon the completion of this process, the bilayer is in the liquid disordered phase.

The minimum at $T_m$ in the lag-time preceding the onset of the activity of phospholipase $A_2$ towards phosphatidylcholines has been attributed to a maximum in the length of the boundary [23]. We suggested the boundary emerging between the coexisting gel and fluid phases to be equivalent to the intermediate phase, being present at $T_m$, with the entire bilayer becoming a "boundary". Contrasting the above, observations on phospholipid Langmuir-films by fluorescence and electron microscopy and AFM studies on Langmuir–Blodgett films, and supported bilayers undergoing phase transition, have revealed large-scale coexistence of gel and fluid phases [26–30], segregated on a scale extending to tens of microns. Importantly, the average diameter of large unilamellar vesicles (LUVs) is approximately 100 nm, requiring domains to be significantly smaller. It is possible that the truly macroscopic dimensions of monolayers, Langmuir–Blodgett films and supported bilayers together with the mica–membrane interactions impose constraints on the transition process so as to alter its nature in a fundamental manner. Such difference is suggested by the contradiction of the above data on planar model membranes and those from X-ray diffraction studies. More specifically, while 'large-scale' coexistence of gel and fluid phases characteristic for a first order transition is seen at low water contents, X-ray studies on fully hydrated DPPC at low scan rates have revealed lack of this two phase region, the transition progressing as a continuous process [31,32]. Tenchov et al. interpreted their data on cooling scans to comply with the presence of an intermediate phase with 'small scale' coexistence. Accordingly, while our model to some extent contrasts the conventional view of phospholipid main phase transition as a strict first order process, it is compatible with X-ray measurements on fully hydrated DPPC.

Our model was mainly derived from the behavior of a pyrene-labelled fluorescent phospholipid derivate 1-palmitoyl-2[10-(pyren-1-yl)]decanoyl-*sn*-glycero-3-phosphocholine (PPDPC) in DMPC [33] and DPPC [1] matrices. It must be emphasized that because the presence of the fluorophore we were observing the transition of an 'impure' DPPC matrix and in essence the mechanism forwarded applies in strict sense to the bilayer melting in the presence of the contained probes [1]. The interpretation of the data involved considerations from hydrophobic mismatch of the above fluorescent probe and the DPPC matrix [1]. To obtain a more complete picture of the phospholipid main transition, we used in this study 1,2-dinervonoyl-*sn*-glycero-3-phosphocholine (DNPC) liposomes ($T_m$ at $\approx 26$ °C) with trace amounts of the fluorescent probe PPDPC. DNPC contains very long 24:1-*cis*15 chains and thus forms significantly thicker bilayers than DPPC. We are not aware of DNPC being found in cellular membranes and this choice was merely dictated from the point of view of being able to clarify the physical basis of the questions addressed in the study, i.e. the role of hydrophobic matching condition. Pyrene-labeled lipids such as PPDPC form excimers (excited dimers) in a concentration-dependent manner [34,35]. In brief, excited pyrene may either relax back to ground state by emitting at $\sim 400$ nm or collide with a ground state pyrene so as to yield an excited dimer, excimer. The latter relaxes back to two ground state

pyrenes while emitting at ~480 nm. In the absence of possible quantum mechanical effects [34], the ratio of excimer and monomer emission intensities ($I_e/I_m$) depends on the collision rate between pyrene moieties. As the efficiency of excimer formation is controlled by both the rate of lateral diffusion and local enrichment [34], pyrene-labeled lipids have been utilized to measure the mobility of lipids [36] as well as the formation of domains [37], and domain boundaries [33,38], in membranes. The variation of $I_e/I_m$ as a function of the content of the probe has been interpreted as the formation of superlattices [39–43], the driving force being steric repulsion between the bulky probe moieties covalently linked to the phospholipid structure. To assess acyl chain order, we measured fluorescence anisotropy for 2-(3-(diphenylhexatrienyl) propanoyl)-1-hexadecanoyl-*sn*-glycero-3-phosphocholine (DPHPC). This phospholipid analog has approximately threefold preference for the fluid relative to the gel phase and it thus reports a lower phase transition temperature as observed by differential scanning calorimetry (DSC) [44]. Transition temperatures and enthalpies were derived from DSC.

## 2. Materials and methods

### 2.1. Materials

HEPES and EDTA were purchased from Sigma, DNPC from Coatsome (Amagasaki, Hyogo, Japan), DPHPC from Molecular Probes (Eugene, OR), and PPDPC from K&V Bioware (Espoo, Finland). No impurities were detected in the above lipids upon thin-layer chromatography and examination of the silicic acid coated plates after iodine staining using chloroform/methanol/water/ammonia (65:20:2:2, by vol.) as the eluent. Lipids were dissolved and stored in chloroform without further purification. Concentration of DNPC was determined gravimetrically using a high precision electrobalance (Cahn Instruments, Cerritos, CA). The concentrations of the labeled lipids were determined spectrometrically for ethanol solutions using a Perkin-Elmer Lambda Bio 40 UV/VIS spectrometer (Norwalk, CT). Molar extinction coefficients of 80,000 $cm^{-1}$ at 356 nm and 42,000 $cm^{-1}$ at 342 nm were employed for DPHPC and PPDPC, respectively. The buffer used in all experiments was 20 mM HEPES, 0.1 mM EDTA, pH 7.0, prepared in freshly deionized Milli RO/Milli Q water (Millipore, Bedford, MA). The pH of the buffer was adjusted to 7.0 with NaOH.

### 2.2. Preparation of liposomes

Lipids were dissolved and mixed in chloroform to yield the indicated compositions. For steady state fluorescence measurements, the lipid analogs PPDPC and DPHPC were included at mole fractions of 0.02 and 0.005, respectively. After mixing of the lipids, the solvent was removed under a gentle stream of nitrogen. The lipid residue was subsequently maintained under reduced pressure for at least 4 h and then hydrated above the main transition temperature of DNPC to yield a lipid concentration of 0.7 mM. Multilamellar vesicles (MLVs) were used as such in the DSC measurements. To obtain unilamellar vesicles the hydrated lipid mixtures were extruded with a LiposoFast small-volume homogenizer (Avestin, Ottawa, Canada) above the transition temperature. Samples were subjected to 19 passes through one polycarbonate filter (100-nm pore size, Nucleopore, Pleasanton, USA). After extrusion, lipid concentrations were verified by gravimetric analysis. Both LUVs and MLVs were annealed by taking them five times through the transition by repeated heating and cooling between zero and 60 °C. Minimal exposure of the lipids to light was ensured throughout the procedure. Subsequently, the liposome solutions were divided into proper aliquots and diluted with the above buffer for DSC and fluorescence spectroscopy. The final total lipid concentrations used in the steady state and time-resolved fluorescence experiments were verified by gravimetric analysis and the corresponding concentrations were 12 and 50 μM, respectively.

### 2.3. DSC

The heating scans were recorded using VP-DSC microcalorimeter (Microcal, Northampton, MA, USA). Heating rate was 30°/h, and the final lipid concentration in the DSC cell was 0.7 mM for MLVs and 0.35 mM for LUVs. Analysis of individual samples was repeated once to verify reproducibility. The obtained endotherms were analyzed using the routines of the software provided by the manufacturer. The transition temperature $T_m$ is by definition the melting point where 50% of the transition is completed and it is thus not necessarily identical to the heat capacity maximum, particularly in the case of strongly asymmetric endotherms. Yet, since the assessment of the underlying molecular level processes was the main aim of this study, we nevertheless for the sake of clarity assign here the heat capacity maximum as the putative $T_m$.

### 2.4. Steady state fluorescence spectroscopy

Steady state fluorescence measurements were carried out with a Varian Cary Eclipse (Palo Alto, CA, USA) spectrofluorometer. Excitation wavelength of 344 and 354 nm were utilised for PPDPC and DPHPC, respectively. Pyrene monomer emission was detected at 398 nm and excimer emission at 480 nm. Fluorescence anisotropy is defined as

$$r = (I_{\parallel} - I_{\perp})/(I_{\parallel} + 2I_{\perp}),$$

where $\parallel$ is the vertical and $\perp$ the horizontal component. Intensity was detected at 428 nm. The cuvette holder of

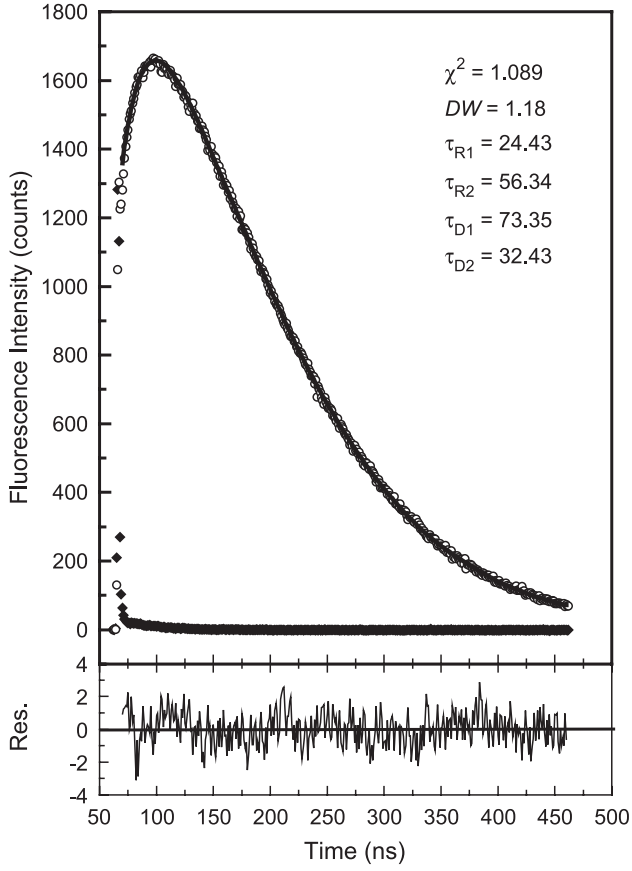


Fig. 1. A typical time-resolved fluorescence intensity profile recorded at 14 °C after the laser pulse, together with its fit and residuals. Also shown are the $\tau_R$ and $\tau_D$ obtained from the fit, with the indicated values for $\chi^2$ and DW.

the spectrofluorometer is equipped with a magnetic stirrer and is thermostated with a circulating water bath. The average scanning rate was about 3 °/h, and the temperature was monitored continuously with a probe placed in a cuvette placed adjacent to the sample cuvette in the holder.

### 2.5. Time-resolved fluorescence spectroscopy

Time-resolved fluorescence measurements were performed with a commercially available system (PTI, Ontario, Canada). A train of 500-ps excitation pulses at 337 nm at a repetition rate of 10 Hz was produced by a nitrogen laser. Time-resolved fluorescence intensities of pyrene monomers and excimers were detected at 398 and 480 nm, respectively by a photomultiplier tube (Hamamatsu, Japan). The minimum lifetime accessible to the instrument is 200 ps. Each intensity decay curve recorded at the indicated temperature represents an average of five subsequent measurements, and the reproducibility of the essential features was checked with another separate sample. The decay curves were fitted to a sum of exponentials and analyzed by the nonlinear least squares method. The data shown were selected based on quality control by chi-square test typically producing a reduced $\chi^2$ value of 0.9–1.2. A representative time-resolved decay together with its fit and residuals is depicted on Fig. 1. The average rate of the temperature increase was $\approx 2°$/h. The monomer and excimer fluorescence lifetimes and rise times were measured at every 2° when $-1 \le (T - T_m) \le 4$ and at every 3° when $(T - T_m) < -1$ and $(T - T_m) > 4$. The instrument is equipped with a magnetic stirrer and a circulating water bath to control the temperature. Temperature was measured continuously by a probe (Omega HH42, Stamford, CT, USA) immersed in a cuvette adjacent to the sample in the cuvette holder of the spectrofluorometer.

## 3. Results and discussion

### 3.1. DSC

Both fluorescent phospholipid analogs used in this study represent substitutional impurities in the DNPC matrix and should thus broaden the melting profile. The effects of the lipid probes on the thermal phase behavior of the DNPC MLVs and LUVs were determined by DSC. Similarly to DPPC [1], the enthalpy peak for neat DNPC MLVs is asymmetric, with 47.4 kJ/mol found at $T < T_m$ and 14.6 kJ/mol above $T_m$. Extrusion of MLVs to yield LUVs decreases the $T_m$ values for both neat DNPC liposomes and those containing the fluorescent lipids (Table 1). Compared to MLVs, the corresponding LUVs exhibit broader endotherms, yet remain asymmetric (Fig. 2). We have previously concluded this broadening to reflect reduced co-operativity and coherence of the membrane due to the lack of interbilayer coupling [45] as well as both increased curvature of the vesicles [11] and smaller size of the LUVs limiting the maximum size of the co-operative unit. The presence of PPDPC ($X_{PPDPC} = 0.01$) in DNPC MLVs lowers $T_m$ from 26.8 to 26.1 °C, with a slight broadening of the peak. Broadening is observed also for MLVs containing DPHPC ($X = 0.005$), with $T_m$ decreasing slightly to 26.7 °C.

Table 1
Values for $T_m$ (in °C) measured by DSC for both MLVs and LUVs with different lipid compositions (in mole fractions, within brackets) and enthalpy (kJ/mol)

| Vesicle composition | MLV | | LUV |
|---|---|---|---|
| | $T_m$ | $\Delta H$ | $T_m$ |
| DNPC | 26.8 | 62 | 25.6 |
| DNPC/PPDPC (0.98:0.02) | 26.5 | 61 | 25.6 |
| DNPC/DPHPC (0.995:0.005) | 26.7 | 61 | 26.4 |

The total lipid concentration in the DSC cell was 0.7 mM for MLVs and 0.35 mM for LUVs in 20 mM HEPES, 0.1 mM EDTA, pH 7.0.

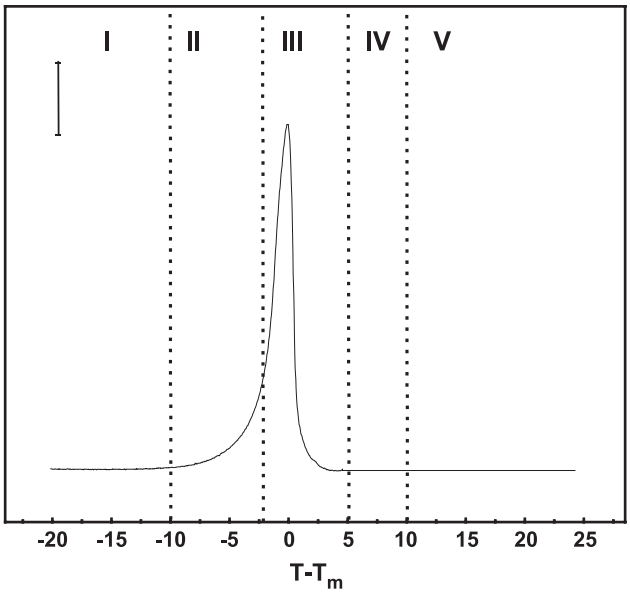


Fig. 2. DSC excess heat capacity scan for DNPC LUVs with $X_{PPDPC} = 0.02$. The calibration bar corresponds to 1 kJ/deg mol$^{-1}$. The total lipid concentration was 0.35 mM in 20 mM HEPES, 0.1 mM EDTA, pH 7.0. The dotted lines mark the peak in heat capacity.

The main phase transition of lamellar lipid bilayers is considered to be a pseudocritical, weakly first-order process [46]. Decrement in $T_m$ by the fluorescent probes could result from their preferential partitioning into the fluid phase or the interfacial boundary between coexisting fluid and gel state domains in the transition region [11–13] as reported earlier for PPDPC in DMPC [33] and DPPC [1]. This enrichment would stabilize the boundary and thus favor the formation of fluid domains at lower temperatures. The decrement in overall transition enthalpy caused by the probes is in keeping with their chain disordering effect at $T < T_m$, thus resulting in smaller remaining increment in the extent of *trans*-→*gauche* isomerization upon chain melting in the transition.

The temperature interval between pre- and main transition is chain-length-dependent [47]. For DPPC it is 7°, whereas for DNPC pretransition merges with the main transition. The transition endotherm is strongly asymmetric and the enthalpy change ($\Delta H$) starts already at $(T - T_m) \sim -10$ (Fig. 2).

### 3.2. Steady state fluorescence spectroscopy

For DNPC–PPDPC ($X_{PPDPC} = 0.01$) LUVs, the values for $I_e/I_m$ increase with temperature up to a local maximum at $(T - T_m) \approx -11$, followed by a decline and a local minimum at about 2° above $T_m$ (Fig. 3). When $(T - T_m) < -11$ or $(T - T_m) > 2$, the value for $I_e$ increases slightly with temperature (Fig. 4A), in keeping with enhanced lateral diffusion. Starting at $(T - T_m) \approx -11$, and upon approaching $T_m$, the value for $I_e$ declines steeply. Values for $I_m$ exhibited changes reciprocal to those for $I_e$ (Fig. 4B). In the gel phase, the pyrene-labeled analog PPDPC thus appears to form clusters so as to minimize the perturbation that it imparts to the packing of the acyl chains of DNPC and resulting in a high $I_e/I_m$ similarly to DPPC [39,43]. Fluorescence anisotropy $r$ of DPHPC assessing acyl chain order decreases with temperature, with the midpoint for the decline at about $(T - T_m) = -0.7$ (Fig. 5).

### 3.3. Time-resolved fluorescence spectroscopy

To obtain more insight into the molecular level processes involved, we measured pyrene monomer lifetimes ($\tau_M$) as well as excimer formation ($\tau_R$) and decay times ($\tau_D$) for PPDPC as a function of temperature. The time-resolved data reveal several discontinuities in the fluorescence kinetics of PPDPC in DNPC, similarly to our previous study on the behavior of this probe in DPPC. The integrated excimer intensity $^{Int}I_e$ of the time-resolved fluorescence emission at 480 nm behaves identically to steady state $I_e$, as expected (Fig. 7). Yet, in the time-resolved temperature scan, $^{Int}I_e$ starts to decrease already at $(T - T_m) \approx -15$, which is likely to reflect the different scanning rates used in the steady state and the time-resolved experiments. To facilitate the interpretation of the data (Figs. 2–8), the time-resolved fluorescence behavior (presented below) in particular, the observed processes were divided into five temperature

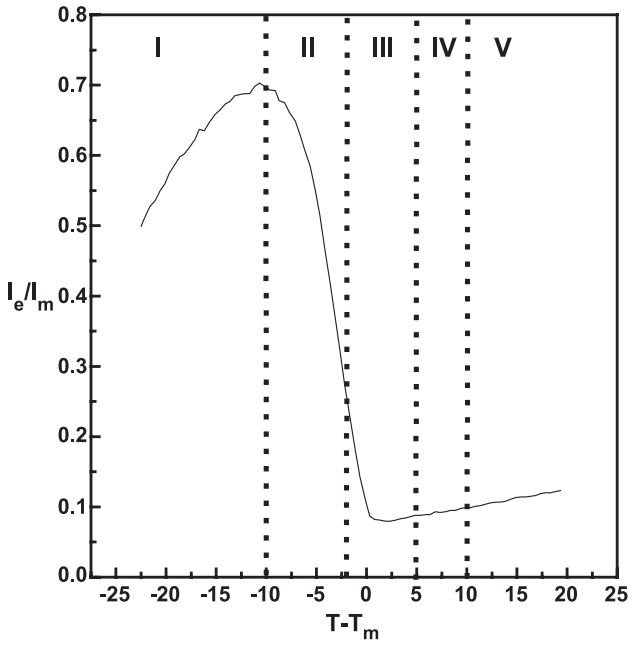


Fig. 3. Ratio of pyrene excimer and monomer steady state emission intensities $I_e/I_m$ for DNPC LUVs at $X_{PPDPC} = 0.02$ as a function of $(T - T_m)$. The total lipid concentration was 12 μM in 20 mM HEPES, 0.1 mM EDTA, pH 7.0.

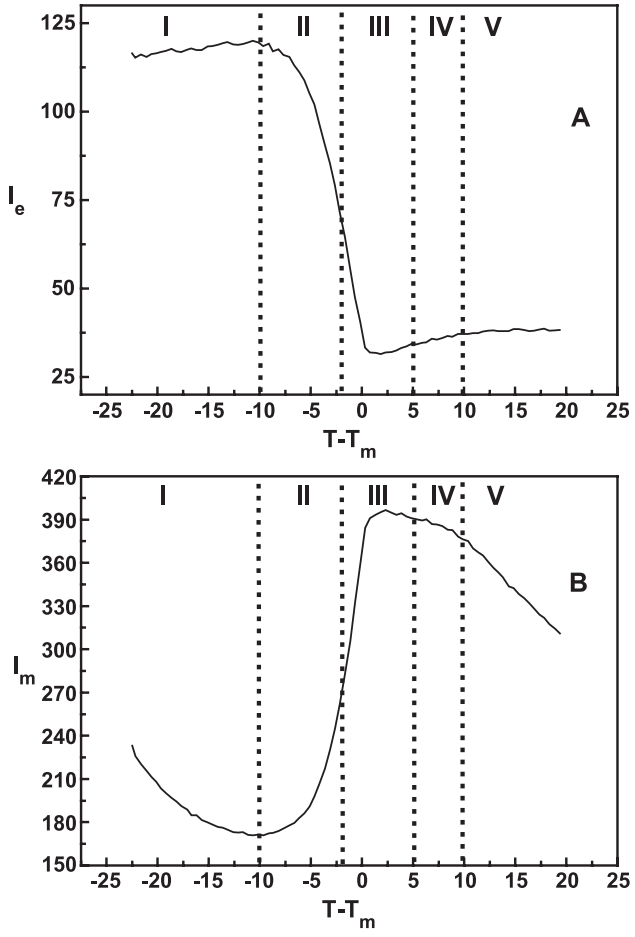


Fig. 4. Excimer (panel A) and monomer (panel B) intensities vs. $(T - T_m)$. The total lipid concentration was 12 μM in 20 mM HEPES, 0.1 mM EDTA, pH 7.0.

ranges separated by four thermally driven transitions, as follows:

$$\text{I}: (T - T_m) < -10$$

$$\text{II}: -10 \leq (T - T_m) < -2$$

$$\text{III}: -2 \leq (T - T_m) < 5$$

$$\text{IV}: 5 \leq (T - T_m) \leq 10$$

$$\text{V}: (T - T_m) > 10$$

In the above, $T_m$ corresponds to the peak of the endotherm detected by DSC for LUVs ($X_{PPDPC} = 0.02$). Due to the scarcity of the data points (limited by practical issues regarding the actual collection of the data), the above temperature ranges should be considered as tentative only, with limits of approximately $\pm 0.5°$.

The kinetics of excimer formation could be best fitted with two rise times of $\tau_{R1}$ and $\tau_{R2}$ varying between 10–22 and 55–72 ns, respectively. The excimer fluorescence decays at 480 nm relax by two processes with decay times $\tau_{D1}$ and $\tau_{D2}$ varying between 57–84 and 10–70 ns, respectively. In region I, the weighted average monomer decay time $\bar{\tau}_M$ decreases together with the excimer formation and decay times ($\tau_R$ and $\tau_D$) (Figs. 6 and 8). The various components used for the fitting raise the question of their possible mixing due to cross-correlation. In this context, we point out that the rise times and the decay times separated by the sign of the pre-exponential factor and the mixing of the individual rise times and decay times, respectively, due to cross-correlation is unlikely because of the difference in both the amplitude of their fluorescence intensity as well as in the absolute values. Yet, because of the inherent characteristics and sensitivity of laser spectroscopy system, it is more reliable to focus on trends revealed by the obtained data, instead of the absolute values and therefore the error bars were not included.

The rise time fractional intensities suggest two PPDPC populations to be present in this temperature range *I*. Because of the high $I_e/I_m$ values observed, the PPDPC probe can be concluded to be enriched in clusters at $(T - T_m) < -9$. The two clustered probe populations present could correspond to (i) PPDPC segregated into clusters within the gel phase DNPC and (ii) PPDPC enriched into line defects separating lamellar sheets of the gel phase

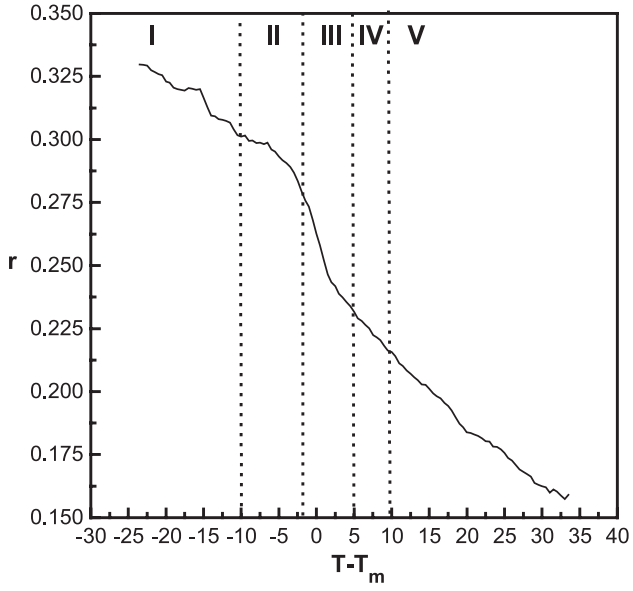


Fig. 5. Anisotropy of DPHPC ($X_{DPHPC} = 0.005$) in DNPC LUVs as a function of $(T - T_m)$. The total lipid concentration was 12 μM in 20 mM HEPES, 0.1 mM EDTA, pH 7.0.

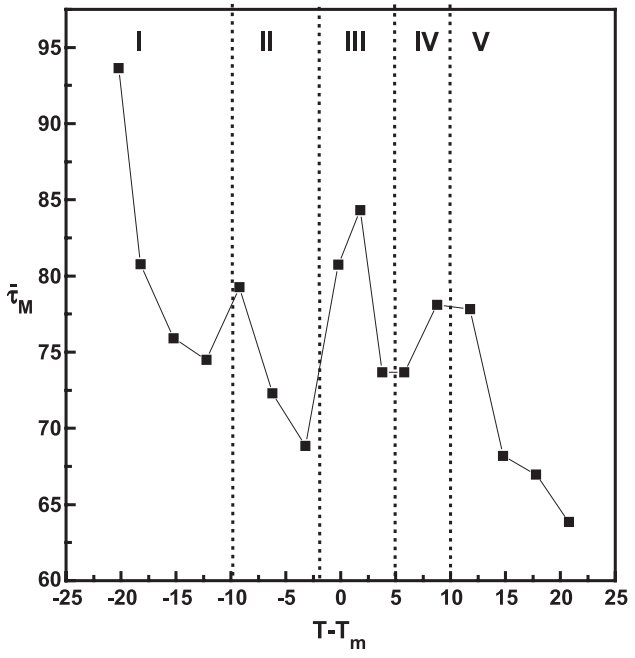


Fig. 6. Weighted average decay time $\bar{\tau}_M$ for monomer emission obtained from time-resolved data for DNPC LUVs with $X_{PPDPC}=0.02$ vs. $(T-T_m)$. The total lipid concentration was 50 μM in 20 mM HEPES, 0.1 mM EDTA, pH 7.0.

DNPC. More specifically, the bending modulus for the long chain DNPC is likely to be small, particularly in the gel state [48]. Accordingly, it is possible that for gel phase DNPC liposomes, their small curvature causes the surface to crack into multiple lamellar regions separated by sharp bends and thus causing line defects where PPDPC would be enriched. The shorter rise time of ~25 ns for PPDPC in the gel phase is quite long and may indicate that excimer formation is not limited by diffusion only but additional, slow rearrangements in the packing of the pyrenyl moieties in a clustered population. It is feasible that also some population of static dimers is involved.

Significant changes in the fractional intensities of the rise time and lifetime components are seen in region I, the fractional intensity of the shorter rise time component ($I_{R1}$) decreasing from its maximum ≈0.43 at $(T-T_m)\approx -20$ to 0.02 at $(T-T_m)\approx -9$. It seems possible that due to softening of the gel phase bilayer, this represents transfer of the pyrene probe from the former type of clusters into the growing line defects. The above changes would be in keeping with pretransition starting at $(T-T_m)\approx -10$, with pseudo one-dimensional defects and corrugations of fluid lipids starting to form [24], in keeping with the decreasing acyl chain order. Simultaneously, $^{Int}I_e$ begins to decrease slightly and the fractional intensity of the shorter decay time ($I_{D2}$) decreases from ≈0.48 at $(T-T_m)\approx -18$ to 0.41 at $(T-T_m)\approx -9$ (Fig. 8A and C). Reciprocal changes are calculated for the fractional intensities of the second components $\tau_{R2}$ and $\tau_{D2}$.

Within the second temperature interval $-10\le(T-T_m)<-2$, the value for the average monomer decay time $\bar{\tau}_M$ first increases to ≈79 ns and then decreases to 68 ns (Fig. 6). A major decrement in the integrated intensity of excimer emission (Fig. 7), reciprocal increase in $I_m$ as well as a decrease in DPHPC anisotropy (Fig. 5) are evident. Despite the continuing decrease in $^{Int}I_e$, the value for $\tau_{R2}$ remains relatively constant until a steep increase and a plateau are reached upon entering into region III (Figs. 7 and 8). More specifically, $^{Int}I_e$ decreases from ≈0.9 at $(T-T_m)=-10$ to ≈0.4 at $(T-T_m)=-1.3$ while $\tau_{R2}$ remains at ≈57 ns. The fractional intensities of $I_{D1}$ and $I_{D2}$ are relatively constant within this range, while $\tau_{D1}$ decreases from ≈68 to 65 ns and $\tau_{D2}$ is slightly prolonged from ≈46 to 48 ns upon $(T-T_m)\rightarrow -2$ (Fig. 8C and D).

The next temperature range of interest is region III between $-1.3\le(T-T_m)\le 5$. This temperature interval coincides with the absorption of a significant fraction (≈50%, corresponding to 31 kJ/mol) of the transition enthalpy for DNPC LUVs ($X_{PPCPC}=0.02$) and the acyl chain melting signaled by DPHPC anisotropy is completed with insignificant changes in $\tau_{R2}$, $\tau_D$, or $^{Int}I_e$. Yet, upon entering this temperature range, there are several pronounced changes in PPDPC fluorescence, as follows. Fractional intensities of both rise time components remain almost constant while $\tau_{R2}$ increases and reaches a local maximum of ≈72 ns at $T_m$. Similar behavior is observed also for the excimer decay times and both $\tau_{D1}$ and $\tau_{D2}$ increase, with insignificant changes in their fractional

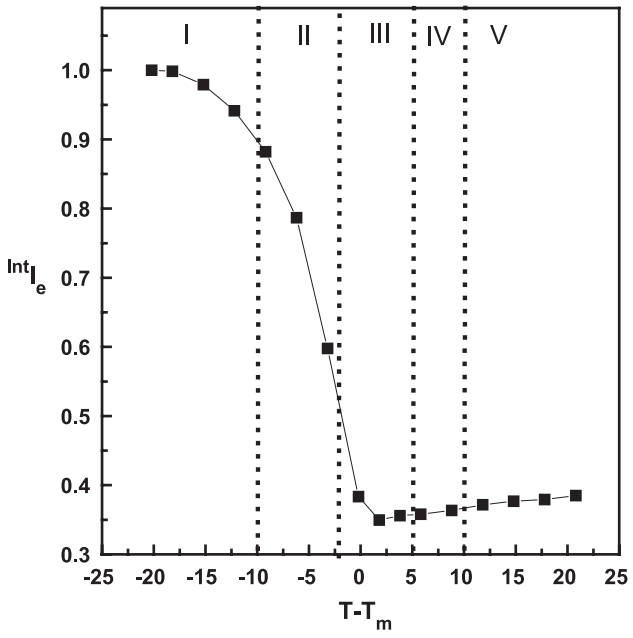


Fig. 7. Integrated PPDPC excimer emission intensity $^{Int}I_e$ vs. $(T-T_m)$ calculated from the time-resolved data for DNPC LUVs with $X_{PPDPC}=0.02$. The data were normalized with respect to the highest $^{Int}I_e$ value. Excitation wavelength was at 337 nm, and emission was recorded at 480 nm. The total lipid concentration was 50 μM in 20 mM HEPES, 0.1 mM EDTA, pH 7.0.

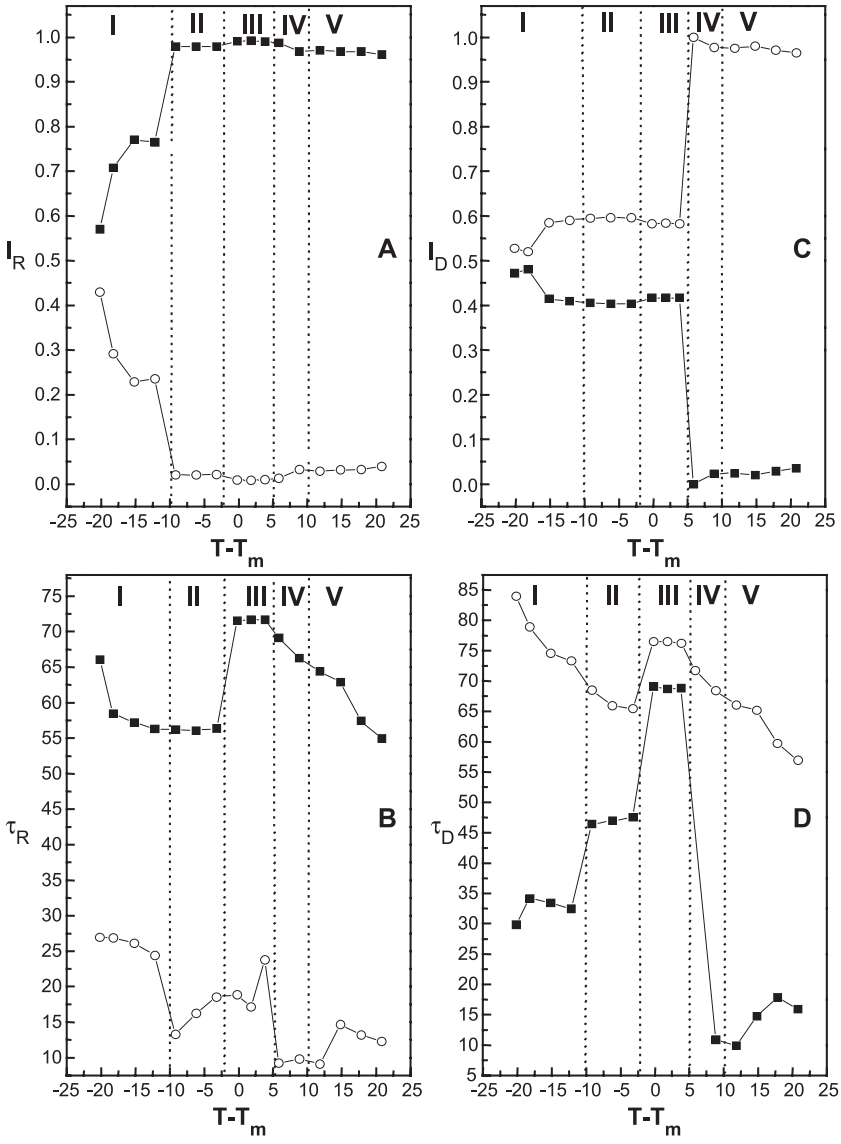


Fig. 8. Excimer fluorescence emission fractional intensities $I_{R1}$ (○) and $I_{R2}$ (■) of the rise times (panel A), and decay times $I_{D1}$ (○) and $I_{D2}$ (■) (panel C) as well as variation of the excimer rise times (panel B), and decay times (panel D) as a function of temperature. See text for details.

intensities. The difference between $\tau_{D1}$ and $\tau_{D2}$ almost vanishes and is only $\approx 5$ ns. We have suggested an intermediate phase to exist in the course of the DPPC main transition consisting of a strongly fluctuating lattice of both fluid-like ("excited") and gel-like ("ground") lipids [1,33]. The above data would be consistent with an intermediate phase occurring also in the course of DNPC main transition in region III. For DNPC, its formation would start at $(T - T_m) \rightarrow -1$ and this phase would prevail until $(T - T_m) \approx 5$. It is likely that the increase in $\tau_{R2}$ upon reaching region III is due to the disappearance of the rippled-like phase and the subsequent redistribution of PPDPC into the bilayer plane. This is suggested also by the low values for $^{Int}I_e$ in region III, in keeping with repulsion between PPDPC molecules [39]. The sudden increments in $\tau_{D1}$ and $\tau_{D2}$ are likely to reflect changes in the local environment surrounding the pyrene moiety, with the fluid bilayer allowing prolongation of excimer decay times.

In the interpretation of our previous studies [1,33] on the behavior of the PPDPC in the course of the main phase transition of DMPC and DPPC, centrally important was hydrophobic mismatch. More specifically, the effective length of the fluorescent phospholipid analog PPDPC exceeds that of DMPC as well as DPPC, although for the latter the difference is less, particularly in the gel state. Importantly, the bulky pyrene moiety makes the probe virtually incompressible along its longest axis. This is contrasted by DPPC, for which increasing extent of *trans* → *gauche* isomerization can decrease the effective length of the molecule. Decrease in the thickness of the matrix lipids occurring in the main transition thus exerts

changes in the interaction potentials of the probe with the matrix, influencing the distribution of the probe determined by the free energy of the system. In order to diminish the above consequences of the hydrophobic mismatch as the driving force determining the distribution of the probe we used DNPC as matrix. There is no decrement in the quantum yield of PPDPC fluorescence, unlike in DPPC [1]. This could be due to the lack of proper type of hydrophobic mismatch between DNPC and PPDPC. Because of the very long acyl chains, the effective length of DNPC exceeds that of PPDPC. However, the conditions are different from those prevailing for PPDPC in DPPC bilayers. This is due to the fact that *trans* → *gauche* isomerization of the terminal ends of the acyl chains of DNPC easily allows this lipid to fill the voids underneath the shorter PPDPC, thus diminishing the impact of the difference in their effective lengths. Obviously, this is not possible for PPDPC in DMPC and DPPC matrices.

Upon entering the fluid phase (range IV) with $(T - T_m)$ exceeding 5, the fractional intensity of the excimer decay component $I_{D1}$ increases to unity and the decay at this point is described by a single exponential process. Accordingly, the kinetics of the decay thus signals the bilayer to be homogeneous at $(T - T_m) \approx 5$. In temperature range IV the weighted monomer decay time $\tau_M$ begins to decrease (Fig. 6). The fractional intensities of $I_{R1}$ and $I_{D1}$ remain nearly constant, the former increasing from $\approx 0.01$ to 0.03 and the latter decreasing from 1 to $\approx 0.98$ (Fig. 8). Changes are no longer evident either in the transition enthalpy or acyl chain order and there are no anomalies in the time-resolved data that would require distinction of regions IV and V. Yet, their presence is suggested by the discontinuities evident in the steady state fluorescence data (Fig. 4). The above changes in the liquid disordered phase bilayer would be in keeping with thermally activated increase in the lateral mobility of the probe. The underlying process remains elusive at this stage. In this connection the model proposed by Kharakoz and Shlyapnikova [25] could be relevant. More specifically, those authors forwarded evidence for small gel state nuclei existing at temperatures well above $T_m$. The fluid–solid interfacial line tension between the gel state nuclei and surrounding fluid phase was proposed to be high enough for the transition to be first-order, and at the same time, weak enough to allow extensive heterophase fluctuations [25]. The time scale for these fluctuations was suggested to be of the order of 10–60 ns, which is very close to the time scale of excimer fluorescence.

## Acknowledgements

The authors wish to thank Dr. Juha-Matti Alakoskela for several rewarding discussions on phospholipid main transition. Technical assistance of Kaija Niva and Kristiina Söderholm is appreciated. HBBG is supported by Finnish Academy and Memphys by The Danish National Research Foundation. A.J.M. acknowledges grants from the Reasearch and Science Foundation of Farmos and Suomen Lääketieteen Säätiö.

## References

[1] A.J. Metso, A. Jutila, J.-P. Mattila, J.M. Holopainen, P.K.J. Kinnunen, Nature of the main transition of dipalmitoylphosphocholine bilayers inferred from fluorescence spectroscopy, J. Phys. Chem., B 107 (2003) 1251–1257.
[2] P.K.J. Kinnunen, P. Laggner (Eds.), Chem. Phys. Lipids 57 (2–3) (1991) 109–408 (Special Issue).
[3] P.K.J. Kinnunen, On the principles of functional ordering in biological membranes, Chem. Phys. Lipids 57 (1991) 375–399.
[4] P.K.J. Kinnunen, O.G. Mouritsen (Eds.), Chem. Phys. Lipids 73 (1–2) (1994) 181–207 (Special Issue).
[5] J.-F. Tocanne, L. Cézanne, A. Lopez, B. Piknova, V. Schram, J.-F. Tournier, M. Welby, Lipid domains and lipid/protein interactions in biological membranes, Chem. Phys. Lipids 73 (1994) 139–158.
[6] O.G. Mouritsen, P.K.J. Kinnunen, Role of lipid organization and dynamics for membrane functionality, in: K.M. Merz, B. Roux (Eds.), Biological Membranes, Birkhäuser, Boston, 1996, pp. 465–504.
[7] R.M. Epand Jr., Studies of membrane physical properties and their role in biological function, Biochem. Soc. Trans. 25 (1997) 1073–1079.
[8] P.K.J. Kinnunen, Lipid bilayers as osmotic response elements, Cell. Physiol. Biochem. 10 (2000) 243–250.
[9] R.F.M. de Almeida, A. Fedorov, M. Prieto, Sphingomyelin/phosphatidylcholine/cholesterol phase diagram: boundaries and composition of lipid rafts, Biophys. J. 85 (2003) 2406–2416.
[10] T.N. Estep, D.B. Mountcastle, Y. Barenholz, R.L. Biltonen, T.E. Thompson, Thermal behaviour of synthetic sphingomyelin–cholesterol dispersions, Biochemistry 18 (1979) 2112–2117.
[11] D. Marsh, A. Watts, P.F. Knowles, Cooperativity of the phase transition in single- and multibilayer lipid vesicles, Biochim. Biophys. Acta 465 (1977) 500–514.
[12] S. Doniach, Thermodynamic fluctuations in phospholipid bilayers, J. Chem. Phys. 68 (1978) 4912–4916.
[13] E. Freire, R. Biltonen, Estimation of molecular averages and equilibrium fluctuations in lipid bilayer systems from the excess heat capacity function, Biochim. Biophys. Acta 514 (1978) 54–68.
[14] O.G. Mouritsen, K. Jørgensen, T. Hønger, Permeability of lipid bilayers near the phase transition, in: E.A. Disalvo, S.A. Simon (Eds.), Permeability and Stability of Lipid Bilayers, CRC Press, Boca Raton, FL, 1995, pp. 137–160.
[15] J.F. Nagle, H.L. Scott, Lateral compressibility of lipid mono- and bilayers. Theory of membrane permeability, Biochim. Biophys. Acta 513 (1978) 236–243.
[16] E. Evans, R. Kwok, Mechanical calorimetry of large dimyristoylphosphatidylcholine vesicles in the phase transition region, Biochemistry 21 (1982) 4874–4879.
[17] M. Bloom, E. Evans, O.G. Mouritsen, Physical properties of the fluid lipid-bilayer component of cell membranes: a perspective, Q. Rev. Biophys. 24 (1991) 293–397.
[18] J.-M. Alakoskela, P.K.J. Kinnunen, Probing phospholipid main phase transition with fluorescence spectroscopy and a surface redox reaction, J. Phys. Chem., B 105 (2001) 11294–11301.
[19] D. Papahadjopoulos, K. Jacobson, S. Nir, T. Isac, Phase transitions in phospholipid vesicles, Fluorescence polarization and permeability measurements concerning the effect of temperature and cholesterol, Biochim. Biophys. Acta 311 (1973) 330–348.
[20] J.A.F. Op den Kamp, Lipid phase transition of phosphatidylglycerol in acholeplasma laidlawii membranes studied with phospholipase A2, Rev. Infect. Dis. 4 (1982) 80–84.

[21] V.M. Maynard, R.L. Magin, F. Dunn, Ultrasonic absorption and permeability for liposomes near phase transition, Chem. Phys. Lipids 37 (1985) 1–12.
[22] M. Menashe, G. Romero, R.L. Biltonen, D. Lichtenberg, Hydrolysis of dipalmitoylphosphatidylcholine small unilamellar vesicles by porcine pancreatic phospholipase A2, J. Biol. Chem. 261 (1986) 5334–5340.
[23] T. Hønger, K. Jørgensen, R.L. Biltonen, O.G. Mouritsen, Systematic relationship between phospholipase A2 activity and dynamic lipid bilayer microheterogeneity, Biochemistry 35 (1996) 9003–9006.
[24] T. Heimburg, A model for the lipid pretransition: coupling of ripple formation with the chain-melting transition, Biophys. J. 78 (2000) 1154–1165.
[25] D.P. Kharakoz, E.A. Shlyapnikova, Thermodynamics and kinetics of the early steps of solid-state nucleation in the fluid lipid bilayer, J. Phys. Chem., B 104 (2000) 10368–10378.
[26] V. von Tscharner, H.M. McConnell, An alternative view of phospholipid phase behavior at the air–water interface. Microscope and film balance studies, Biophys. J. 36 (1981) 409–419.
[27] R.D. Neuman, D. Fereshtehkhou, R. Ovalle, Electron microscopic observation of LE/LC phase transition in dipalmitoylphosphatidylcholine monolayers, J. Colloid Interface Sci. 101 (1984) 309–313.
[28] H.M. McConnell, D.J. Keller, Finite two-dimesional phospholipid crystals, Proc. Natl. Acad. Sci. U. S. A. 84 (1987) 4706–4708.
[29] L.K. Nielsen, T. Bjørnholm, O.G. Mouritsen, Critical phenomena: fluctuations caught in the act, Nature 404 (2000) 352.
[30] F. Tokumasu, A.J. Jin, J.A. Dvorak, Lipid membrane phase behaviour elucidated in real time by controlled environment atomic force microscopy, J. Electron Microsc. 51 (2002) 1–9.
[31] B.G. Tenchov, H. Yao, I. Hatta, Time-resolved X-ray diffraction and calorimetric studies at low scan rates: I. Fully hydrated dipalmitoylphosphatidylcholine (DPPC) and DPPC/water/ethanol phases, Biophys. J. 56 (1989) 757–768.
[32] M. Caffrey, G. Fanger, R.L. Magin, J. Zhang, Kinetics of the premelting ($L\beta'$-$P\beta'$) and main phase transition ($P\beta'$-$L\beta$) in hydrated dipalmitoylphosphatidylcholine. A time-resolved X-ray diffraction study using microwave-induced temperature jumps, Biophys. J. 58 (1990) 677–686.
[33] A. Jutila, P.K.J. Kinnunen, Novel features of the main transition of dimyristoylphosphocholine bilayers revealed by fluorescence spectroscopy, J. Phys. Chem., B 101 (1997) 7635–7640.
[34] P.K.J. Kinnunen, A. Kõiv, P. Mustonen, Pyrene-labeled lipids as fluorescent probes in studies on biomembranes and membrane models, in: O.S. Wolfbeis (Ed.), Fluorescence Spectroscopy, Springer-Verlag, Berlin, 1993, pp. 159–171.
[35] G. Duportail, P. Lianos, Fluorescence probing of vesicles using pyrene and pyrene derivatives, in: M. Rosoff (Ed.), Vesicles, Marcel Decker, New York, 1996, pp. 296–372.
[36] H.-J. Galla, U. Theilen, W. Hartmann, Transversal mobility in bilayer membrane vesicles: use pyrene lecithin as optical probe, Chem. Phys. Lipids 23 (1979) 239–251.
[37] J.Y.A. Lehtonen, J.M. Holopainen, P.K.J. Kinnunen, Evidence for the formation of microdomains in lipid crystalline large unilamellar vesicles caused by hydrophobic mismatch of the constituent phospholipids, Biophys. J. 70 (1996) 1753–1760.
[38] T. Söderlund, A. Jutila, P.K.J. Kinnunen, Binding of adriamycin to liposomes as a probe for membrane lateral organization, Biophys. J. 76 (1999) 896–907.
[39] P.J. Somerharju, J.A. Virtanen, K.K. Eklund, P. Vainio, P.K.J. Kinnunen, 1-Palmitoyl-2-pyrenedecanoyl glycerophospholipids as membrane probes: evidence for regular distribution in liquid-crystalline phosphatidylcholine bilayers, Biochemistry 24 (1985) 2773–2781.
[40] P.K.J. Kinnunen, A. Tulkki, H. Lemmetyinen, J. Paakkola, J.A. Virtanen, Characteristics of excimer formation in Langmuir–Blodgett assemblies of 1-palmitoyl-2-pyrenedecanoylphosphatidylcholine and dipalmitoylphosphatidylcholine, Chem. Phys. Lett. 136 (1987) 539–545.
[41] D. Tang, P.L.-G. Chong, E/M dips: evidence of lipids regularly distributed into hexagonal super-lattices in pyrene-PC/DMPC binary mixtures at specific concentrations, Biophys. J. 63 (1992) 903–910.
[42] I.P. Sugar, D. Tang, P.L.-G. Chong, Monte Carlo simulation of lateral distribution of molecules in a two-component lipid membrane. Effect of long-range repulsive interactions, J. Phys. Chem., B 98 (1994) 7201–7210.
[43] P.L.-G. Chong, D. Tang, I.P. Sugar, Exploration of physical principles underlying lipid regular distribution: effect of pressure, temperature and radius of curvature on E/M dips in pyrene-labeled PC/DMPC binary mixtures, Biophys. J. 66 (1994) 2029–2038.
[44] L. Davenport, Fluorescence probes for studying membrane heterogeneity, Methods Enzymol. 278 (1997) 487–512.
[45] T.I. Lotta, J.A. Virtanen, P.K.J. Kinnunen, Fourier transform infrared study on the thermotropic behaviour of fully hydrated 1-palmitoyl-2-[10-(pyren-1-yl)decanoyl]-*sn*-glycero-3-phosphatidylcholine, Chem. Phys. Lipids 46 (1987) 13–23.
[46] O.G. Mouritsen, Theoretical models of phospholipid phase transitions, Chem. Phys. Lipids 57 (1991) 179–194.
[47] K. Jørgensen, Calorimetric detection of a sub-main transition in long-chain phosphatidylcholine lipid bilayers, Biochim. Biophys. Acta 1240 (1995) 111–114.
[48] T. Heimburg, Mechanical aspects of membrane thermodynamics. Estimation of mechanical properties of lipid membranes close to the chain melting transition from calorimetry, Biochim. Biophys. Acta 1415 (1998) 147–162.